

Supporting Information

Experimental Sections

Synthesis of MXene nanosheets: Firstly, 1 g of lithium fluoride powder was dissolved in 10 mL of concentrated hydrochloric acid (~12 M) under magnetic stirring. Then 1 g of Ti_3AlC_2 powder was added to the above solution gently and the resulting mixture was placed in the pre-prepared thermostatic water bath of 35 °C for 24 h under magnetic stirring. The consequent mixture was rinsed with deionized water and centrifuged at 3500 rpm repeatedly until the pH of the supernatant was close to neutrality. With gentle sonication, the supernatant containing MXene nanosheets was collected after centrifugation. MXene powder could be obtained through lyophilization.¹

Synthesis of MoS_2 nanotubes: MoS_2 nanotubes were prepared via a hydrothermal method in the light of previous reports.² Generally, 76.8 mg of sulphur powder and 185.8 mg of ammonium molybdate were dissolved in the mixed solution of octylamine (28 mL) and absolute ethanol (24 mL) under magnetic stirring for 1 h. Subsequently, the mixture was transferred to a 100 mL Teflon-lined autoclave, sealed, and kept at the thermostatic oven of 200 °C for 24 h. After natural cooling, the consequent mixture was washed with absolute ethanol and deionized water several times. The final product was collected through lyophilization.

Synthesis of MnO_2 nanowires: MnO_2 nanowires were prepared via the hydrothermal reaction according to the previous report.³ Basically, 0.45 g of potassium permanganate powder, 1 mL of concentrated hydrochloric acid (~12 M) and 40 mL deionized water were blended under magnetic stirring for 30 min. Then the above aqueous dispersion was transferred to a 100 mL Teflon-lined autoclave, sealed and kept at 160 °C for 12 h. The resulting mixture was filtered, washed with deionized water and dried at 60 °C overnight.

Preparation of MXene/ MoS_2 composite films: Generally, the dilute aqueous dispersions (~0.5 mg mL⁻¹) of MXene nanosheets and MoS_2 nanotubes were prepared separately under gentle sonication. Subsequently, the above dispersions were added dropwise on the filter membrane alternatively according to different mass ratios (MXene: MoS_2 =1:2, 1:3 and 1:4, denoted as MXene/ MoS_2 -1:2, MXene/ MoS_2 -1:3 and MXene/ MoS_2 -1:4). After vacuum filtration, the membranes were stored under vacuum overnight. The flexible MXene-bonded MoS_2 films were readily peeled off the filter membranes and could serve as LIB anodes directly with no other binder, conductive agent or current collector. For comparison, the neat MXene and MXene-bonded MnO_2 films were fabricated via the similar procedures. Specifically, the mass of all above-prepared films are set as 15 mg, give or take.

Electrochemical measurements: The as-prepared films were tailored to round electrode with a diameter of 12 mm. To evaluate the electrochemical performance, 2025 coin-type half cells were assembled in the argon-filled glove box using lithium

foils as the counter electrodes and 1 M LiPF₆ dissolved in ethylene carbonate/diethyl carbonate (volume ratio=1:1) as electrolyte. In comparison, either neat MoS₂ or MnO₂ powder was made into working electrode slurry containing MoS₂ or MnO₂, acetylene black and poly(vinylidene fluoride) dissolved in N-methyl-2-pyrrolidone with a mass ratio of 8:1:1 at room temperature. The consequent slurry was coated on copper foils and held in vacuum at 120 °C overnight to acquire the slice electrodes. All the galvanostatic charge/discharge (GCD) profiles were measured between 0.01–3 V (vs. Li/Li⁺) via Neware battery test system. Cyclic voltammetry (CV) tests were carried out at a scan rate of 0.1 mV s⁻¹ with the CHI 660d electrochemical workstation. The electrochemical impedance spectroscopy (EIS) tests were conducted within the frequency range of 100000-0.1 Hz utilizing a Parstat 2273 Advanced Electrochemical Systems apparatus.

Characterizations: The powder X-ray diffraction (XRD) measurements were recorded through a PANalytical X'pert PRO X-ray diffractometer with Cu K α radiation ($\lambda=0.154$ nm). Brunauer-Emmett-Teller (BET) tests were measured on the ASAP 2020 adsorption analyser at 77K. The scanning electron microscope (SEM) images were obtained by utilizing a Hitachi SU8000 microscope. Transparent electron microscopy (TEM) and high-resolution transparent electron microscopy (HRTEM) were conducted with a JEOL JEM-2100 microscope. Raman spectra were carried out using a Renishaw confocal Raman spectrometer ($\lambda=633$ nm). X-ray photoelectron spectroscopy (XPS) was evaluated by a Thermo Scientific K-Alpha spectrometer.

Supplementary Figures and Tables

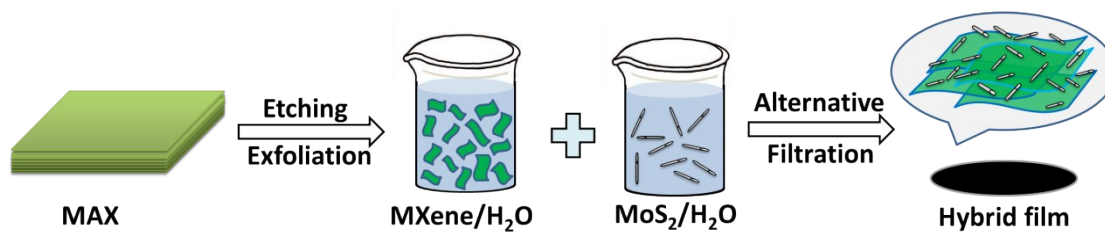


Fig. S1 Schematic illustration of the fabrication procedures of MXene/MoS₂ composite films.

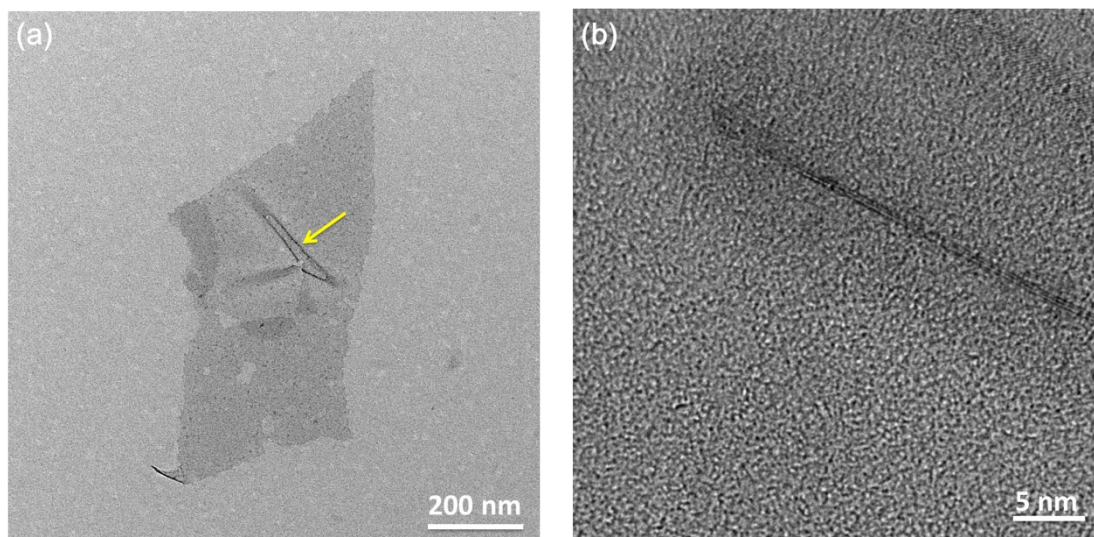


Fig. S2 (a) TEM and (b) HRTEM images of MXene.

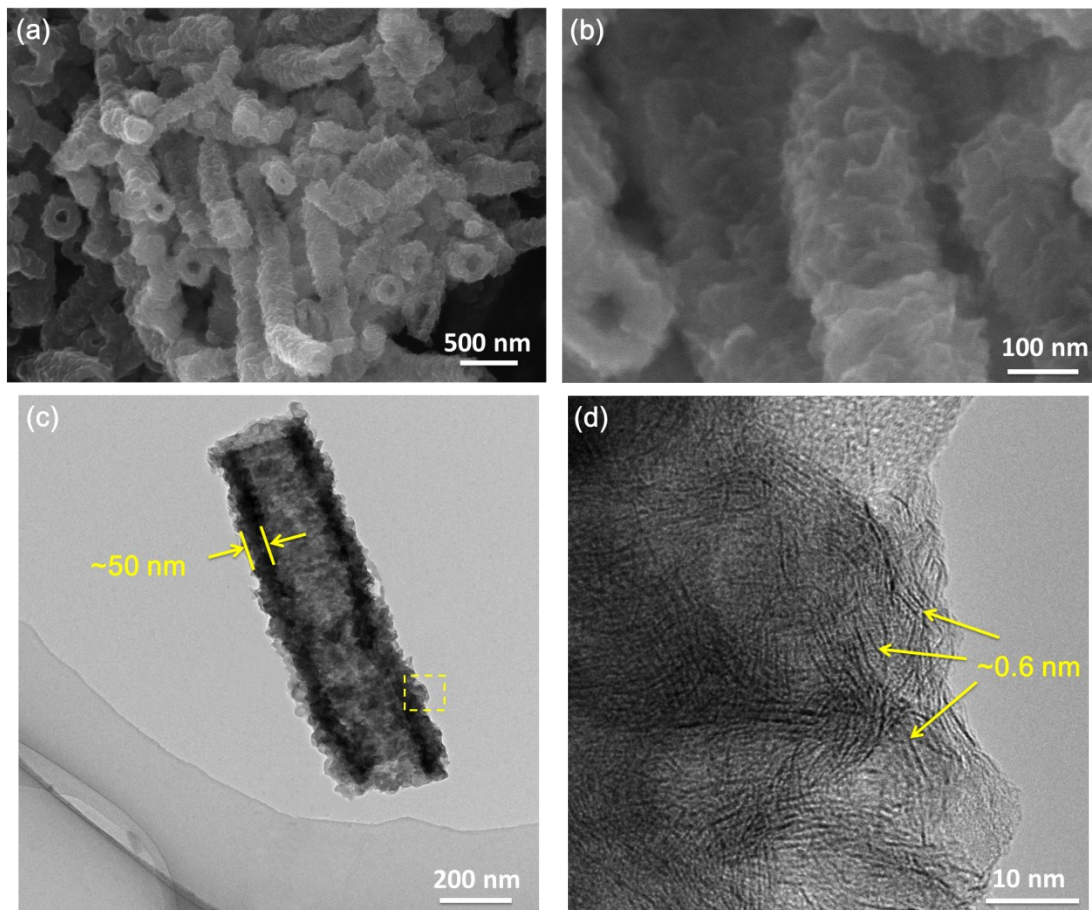


Fig. S3 (a) SEM and (b) corresponding detailed morphology, (c) TEM and (d) HRTEM images of MoS_2 nanotubes.

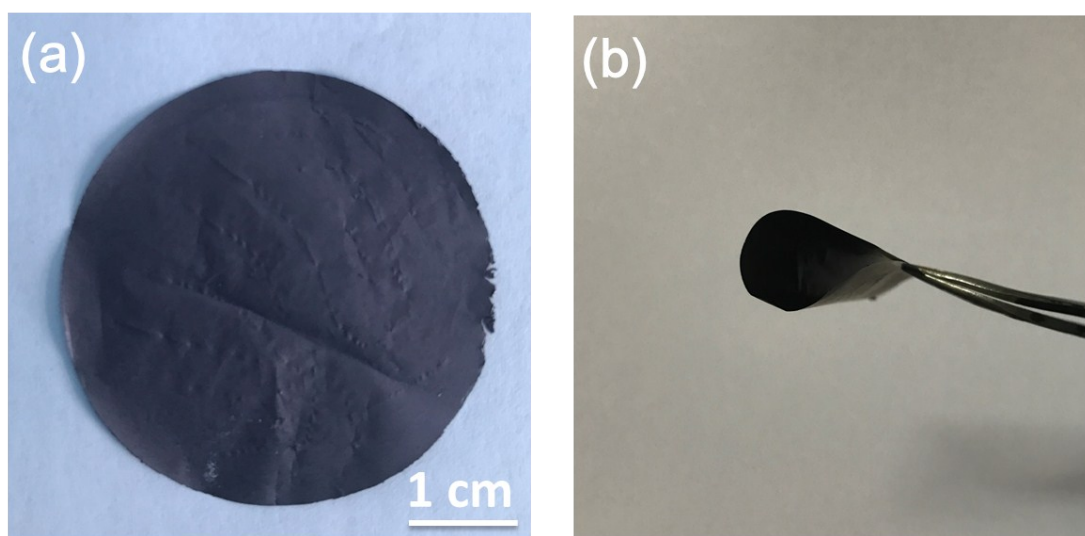


Fig. S4 (a) Macroscopic image of MXene/ MoS_2 -1:3 film, which exhibits superior flexibility (b).

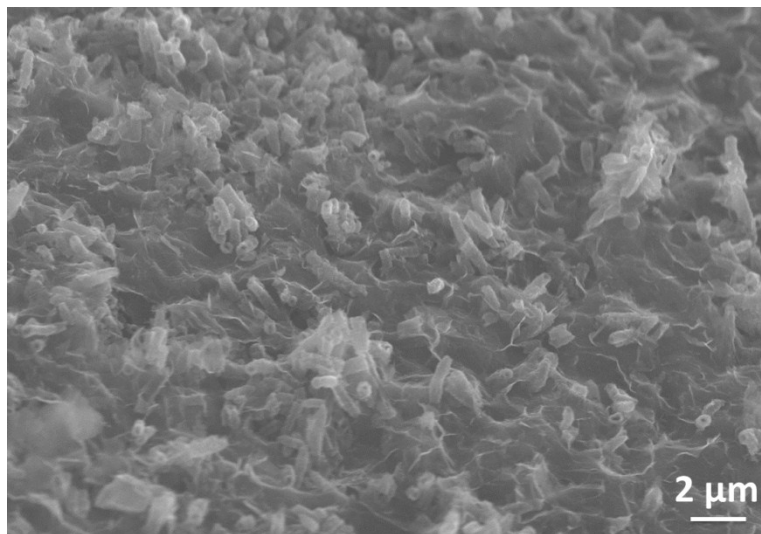


Fig. S5 Top-view SEM image of MXene/MoS₂-1:3 film.

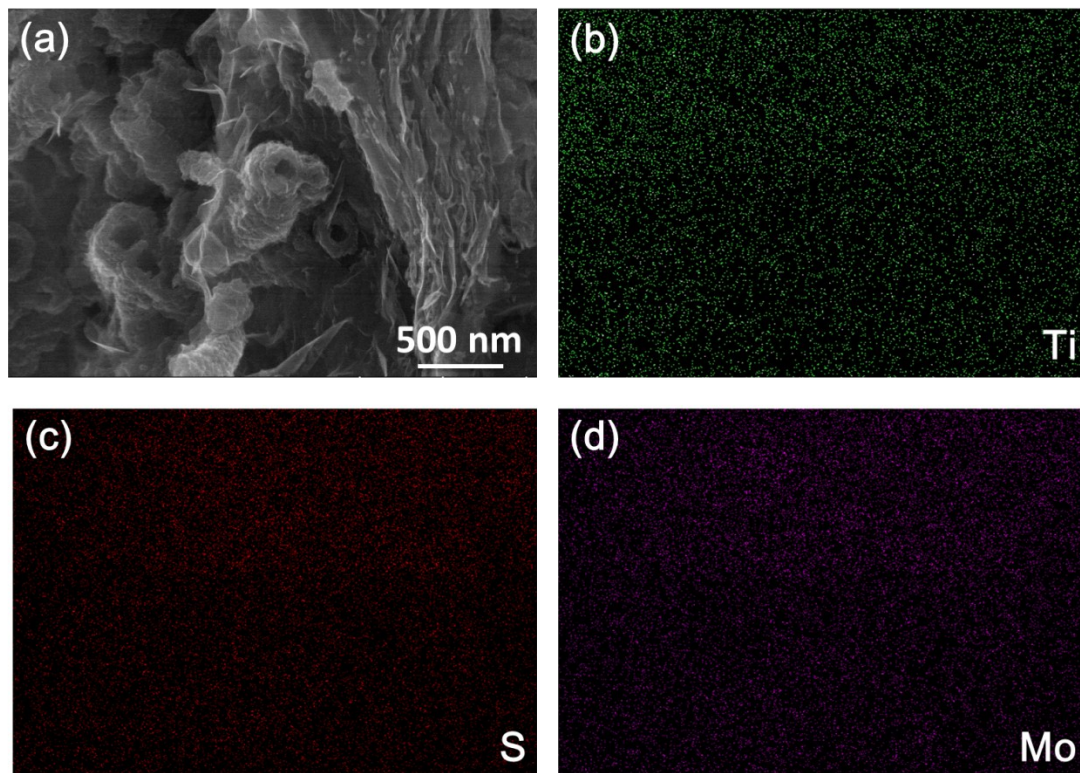


Fig. S6 SEM image of (a) MXene/MoS₂-1:3 and corresponding element mapping validating the uniform distribution of (b) Ti, (c) S and (d) Mo.

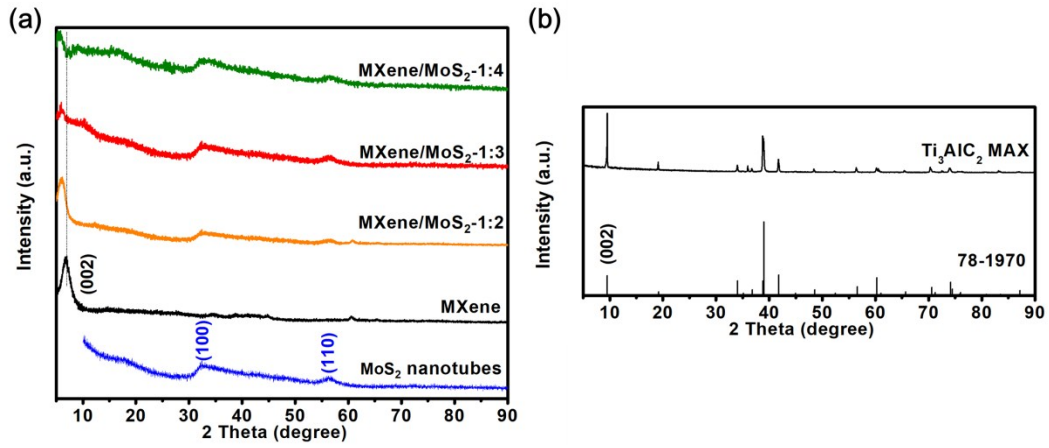


Fig. S7 XRD patterns of (a) MoS₂ nanotubes, MXene nanosheets, composite films at different mass ratios and (b) MAX precursor and corresponding PDF card.

Table S1 Basic physical parameters of MXene, MoS₂ and composite films.

Samples	(002)/degree	d-spacing/(Å)	film thickness/(μm)	SSA/(m ² g ⁻¹)
neat MXene film	6.9	12.8	4.1	25.5
MXene/MoS ₂ - 1:2	6.1	14.4	6.1	39.1
MXene/MoS ₂ - 1:3	5.9	14.9	8.6	41.2
MXene/MoS ₂ - 1:4	5.8	15.2	10.7	44.1
MoS ₂	-	-	-	57.5

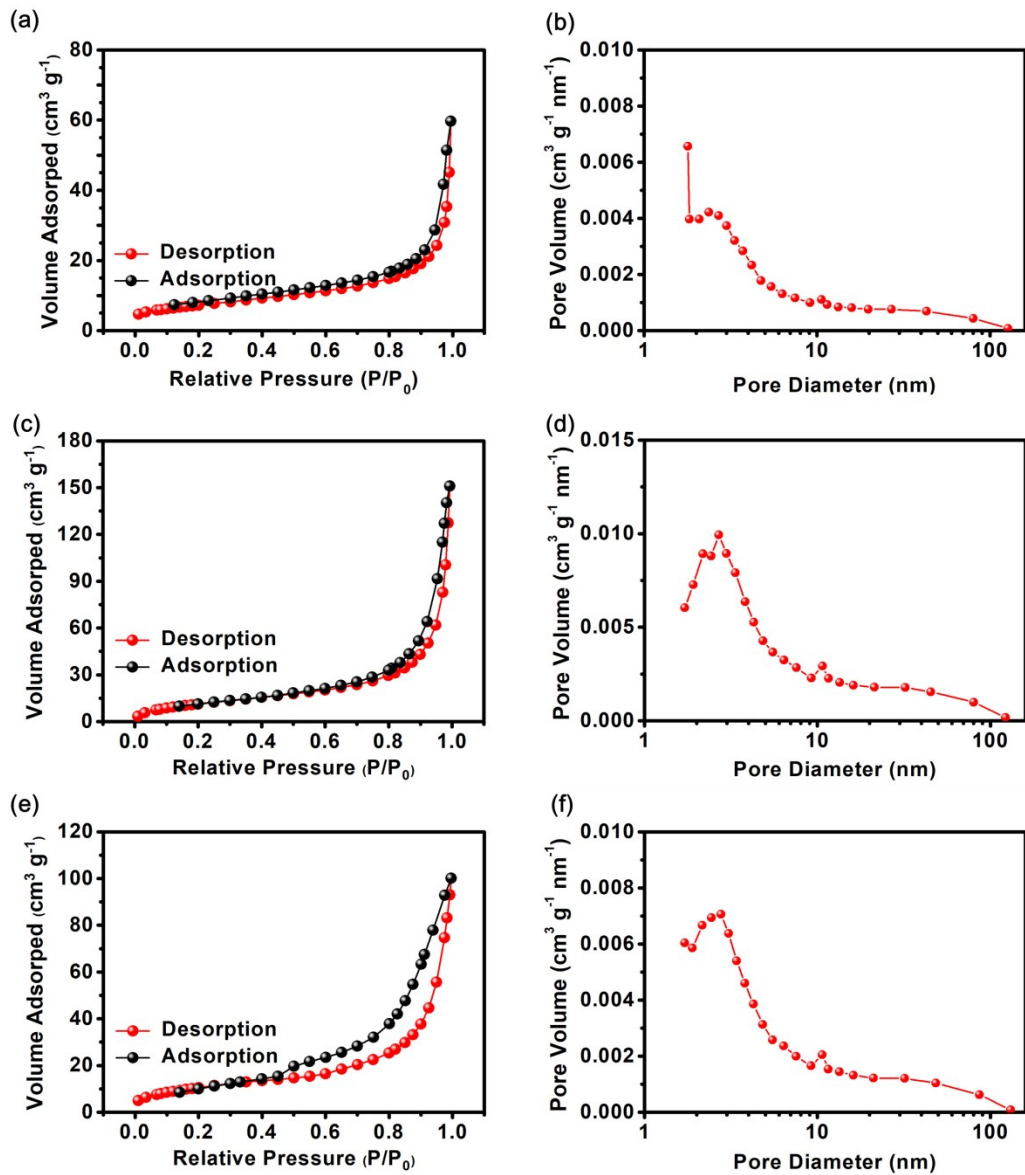


Fig. S8 Nitrogen adsorption-desorption isotherms of (a) MXene film, (c) MoS_2 powder and (e) MXene/ MoS_2 -1:3 composite film and corresponding pore size distribution (b), (d) and (f).

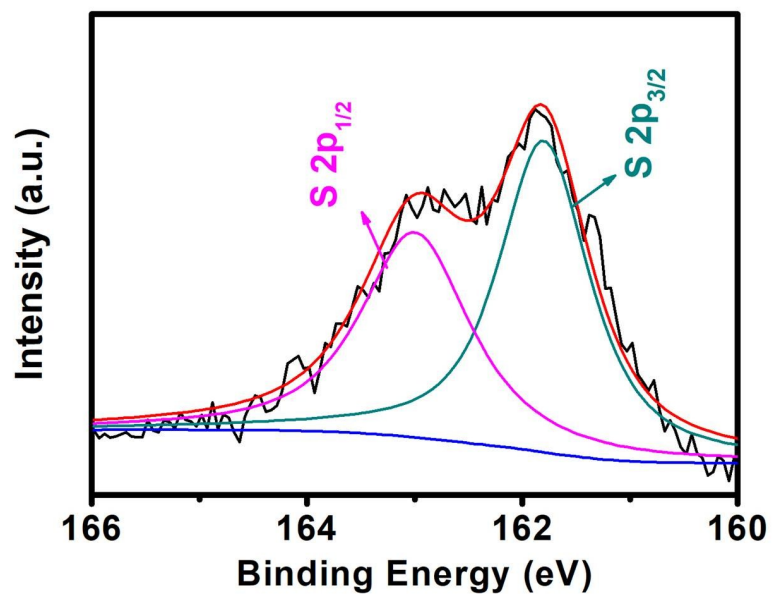


Fig. S9 S 2p spectrum of MXene/MoS₂-1:3 film.

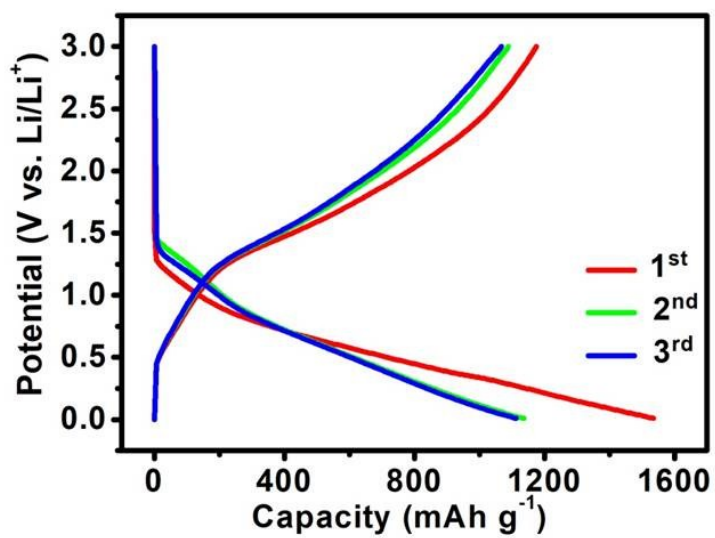


Fig. S10 Charge-discharge curves of MXene/MoS₂-1:3 film at 500 mA g⁻¹.

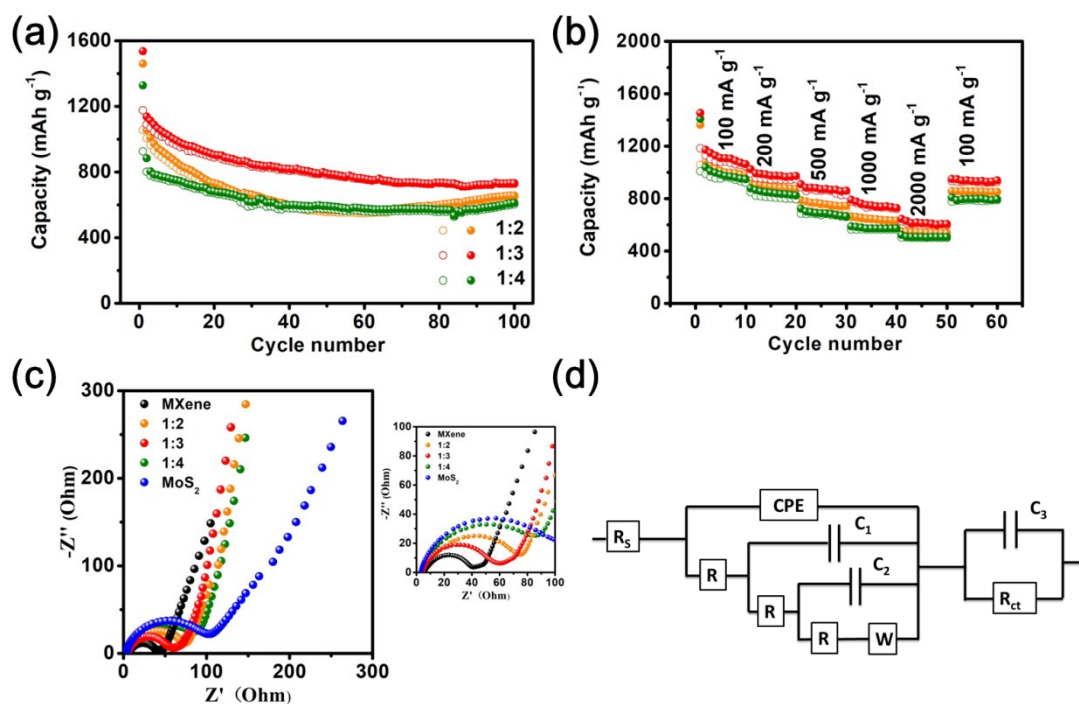


Fig. S11 (a) Cycle performance, (b) rate capabilities, (c) Nyquist plots of MXene/MoS₂ hybrids at different mass ratios and (d) corresponding equivalent circuit of MXene/MoS₂-1:3.

Table S2 The cycle and rate performances of our MXene/MoS₂ hybrid films and previously reported other MoS₂-based and MXene-based anodes.

Samples	Specific capacity (mAh g ⁻¹) (cycling numbers) (current density)	High rate capacity (mAh g ⁻¹)	Reference
MXene/MoS ₂ -1:3	731.0 (100) (0.75C, 1C=670 mA g ⁻¹)	605.4 (2.98 C)	This work
MXene/MoS ₂ -1:3	735.8 (500) (2.98 C)	-	This work
MoS ₂ /CFs	630 (400) (2,39 C)	465.5 (9.55 C)	4
MoS _x /MWNTs	1000 (45) (0.07 C)	197 (2.98 C)	5
single-layered MoS ₂ - carbon nanofiber	600 (1000) (14.92 C)	373 (74.63 C)	6
MoS ₂ /graphene	877 (50) (0.15 C)	466 (5.97 C)	7
MoS ₂ /PEO/graphene	950 (185) (0.07 C)	210 (14.92C)	8
MoS ₂ /polyaniline nanowires	748 (50) (0.15 C)	320 (1.49C)	9
Ti ₃ C ₂ paper	410 (100) (0.48 C)	-	10
Ti ₃ C ₂ /CNTs	428 (300) (0.24 C)	218.2 (0.96 C)	11
PVP-Sn(IV)@Ti ₃ C ₂	544 (200) (0.84 C)	233 (4.48C)	12

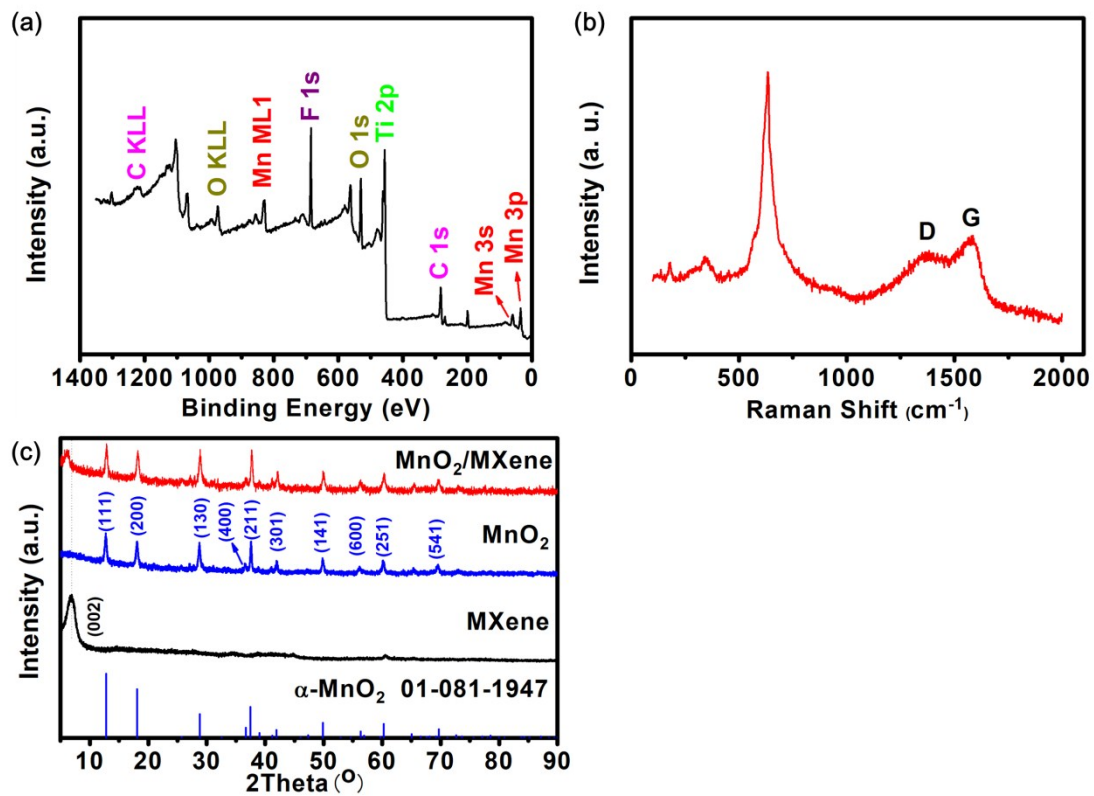


Fig. S12 (a) XPS, (b) Raman and (c) XRD analysis of MXene/ MnO_2 film.

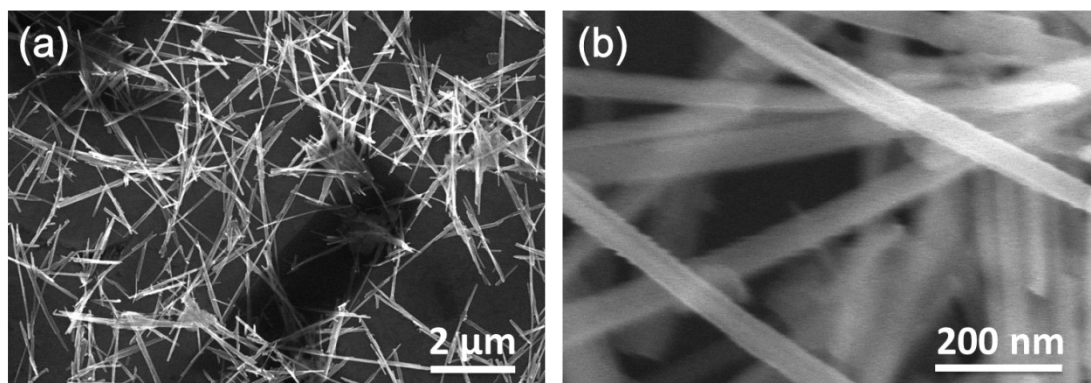


Fig. S13 (a) SEM image and (b) detailed morphology of MnO_2 nanowires.

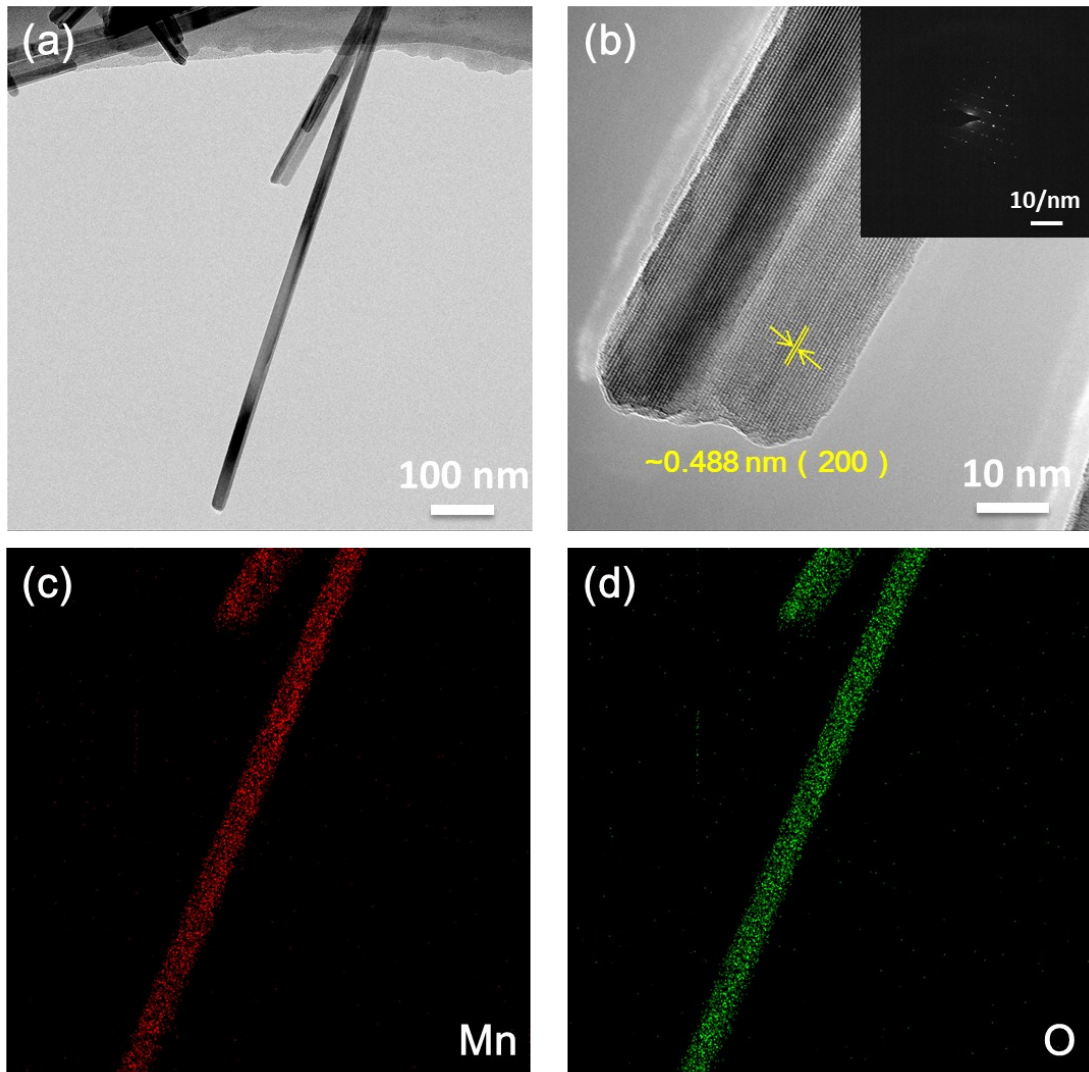


Fig. S14 (a) TEM and (b) HRTEM images of MnO₂ nanowires with inset of SAED; corresponding element mapping validates the uniform distribution of Mn (c) and O (d).

Supporting References

- 1 (a) M. Ghidui, M. R. Lukatskaya, M. Q. Zhao, Y. Gogotsi and M. W. Barsoum, *Nature*, 2014, **516**, 78; (b) C. Wang, X. D. Zhu, Y. C. Mao, F. Wang, X. T. Gao, S. Y. Qiu, S. R. Le and K. N. Sun, *Chem. Commun.*, 2019, **55**, 1237.
- 2 (a) P. P. Wang, H. Y. Sun, Y. J. Ji, W. H. Li and X. Wang, *Adv. Mater.*, 2014, **26**, 964; (b) X. D. Zhu, K. X. Wang, D. J. Yan, S. R. Le, R. J. Ma, K. N. Sun and Y. T. Liu, *Chem. Commun.*, 2015, **51**, 11888.
- 3 C. Tanggarnjanavalukul, N. Phattharasupakun, K. Kongpatpanich and M. Sawangphruk, *Nanoscale*, 2017, **9**, 13630.
- 4 D. Y. Ren, Y. J. Hu, H. B. Jiang, Z. N. Deng, S. Petr, H. Jiang and C. Z. Li, *ACS Sustainable Chem. Eng.*, 2016, **4**, 1148.
- 5 Y. M. Shi, Y. Wang, J. I. Wong, A. Y. S. Tan, C. L. Hsu, L. J. Li, Y. C. Lu and H. Y. Yang, *Sci. Rep.*, 2013, **3**, 2169.
- 6 C. B. Zhu, X. K. Mu, P. A. van Aken, Y. Yu and J. Maier, *Angew. Chem., Int. Ed.*, 2014, **53**, 2152.
- 7 X. H. Cao, Y. M. Shi, W. H. Shi, X. H. Rui, Q. Y. Yan, J. Kong and H. Zhang, *Small*, 2013, **9**, 3433.
- 8 J. Xiao, X. J. Wang, X. Q. Yang, S. D. Xun, G. Liu, P. K. Koech, J. Liu and J. P. Lemmon, *Adv. Funct. Mater.*, 2011, **21**, 2840.
- 9 L. C. Yang, S. N. Wang, J. J. Mao, J. W. Deng, Q. S. Gao, Y. Tang and O. G. Schmidt, *Adv. Mater.*, 2013, **25**, 1180.
- 10 O. Mashtalir, M. Naguib, V. N. Mochalin, Y. Dall'Agnese, M. Heon, M. W. Barsoum and Y. Gogotsi, *Nat. Commun.*, 2013, **4**, 1716.
- 11 Y. Liu, W. Wang, Y. Ying, Y. Wang and X. Peng, *Dalton Trans.*, 2015, **44**, 7123.
- 12 J. Luo, X. Tao, J. Zhang, Y. Xia, H. Huang, L. Zhang, Y. Gan, C. Liang and W. Zhang, *ACS Nano*, 2016, **10**, 2491.